Bioactive Materials 6 (2021) 4517–4530

Contents lists available at ScienceDirect

Bioactive Materials

journal homepage: www.sciencedirect.com/journal/bioactive-materials

Calcium phosphate-based materials regulate osteoclast-mediated osseointegration

Xiaogang Wang [a,c], Yuanman Yu [a,c], Luli Ji [a,c], Zhen Geng [a,c,**], Jing Wang [a,b,*], Changsheng Liu [a,c,d,***]

[a] Key Laboratory for Ultrafine Materials of Ministry of Education, East China University of Science and Technology, Shanghai, 200237, PR China
[b] The State Key Laboratory of Bioreactor Engineering, East China University of Science and Technology, Shanghai, 200237, PR China
[c] Engineering Research Center for Biomedical Materials of the Ministry of Education, East China University of Science and Technology, Shanghai, 200237, PR China
[d] Frontiers Science Center for Materiobiology and Dynamic Chemistry, East China University of Science and Technology, Shanghai, 200237, PR China

ARTICLE INFO

Keywords:
Calcium phosphate-based materials
Osseointegration
Osteoclast
Bone regeneration

ABSTRACT

Calcium phosphate-based materials (CaP) have been widely used as bone graft substitutes with a decent osseointegration. However, the mechanism whereby cells function and repair the bone defect in CaP microenvironment is still elusive. The aim of this study is to find the mechanism how osteoclast behaviors mediate bone healing with CaP scaffolds. Recent reports show that behaviors of osteoclast are closely related with osteogenesis, thus we make a hypothesis that active osteoclast behaviors induced by CaP facilitate bone healing. Here, we found a new mechanism that CaP can regulate osteoclast-mediated osseointegration. Calcium phosphate cement (CPC) is selected as a representative CaP. We demonstrate that the osteoclast-mediated osseointegration can be strongly modulated by the stimulation with CaP. An appropriate Ca/P ratio in CaP can effectively promote the RANKL-RANK binding and evoke more activated NF-κB signaling transduction, which results in vigorous osteoclast differentiation. We observe significant improvement of bone healing *in vivo,* owing to the active coupling effect of osteoclasts. What is more noteworthy is that the phosphate ions released from CaP can be a pivotal role regulating osteoclast activity by changing Ca/P ratio readily in materials. These studies suggest the potential of harnessing osteoclast-mediated osteogenesis in order to develop a materials-manipulated approach for improving osseointegration.

1. Introduction

Bone substitute biomaterials have been proposed as therapeutic strategies to apply for bone regeneration [1], wherein calcium phosphate-based materials (CaP) are widely concerned owing to their excellent biological compatibility and physiochemical property [1,2], which contributes to the excellent osseointegration [3,4]. Osseointegration is a process that responds to implants and adjacent bone matrix, which is always involved in osteogenesis and bone remodeling. Great efforts have been attempted to promote bone healing through mesenchymal stem cells (MSCs)-mediated osteogenesis, such as enhanced proliferation and recruitment of MSCs [5–8], but the clinical effect of bone healing was unsatisfactory. The incomplete osseointegration of bone-material can generate serious postoperative complications including infectious disease [9], implant failure [10], bone nonunion [11], sharper pain [12].

Both osteoclasts and osteoblasts are critical for successful bone osseointegration. Osteoblasts, derived from bone marrow stromal cells, are bone-forming cells and play a vital role in bone formation, maintenance, and remodeling [13,14]. Osteoclasts belong to the lineage of

Peer review under responsibility of KeAi Communications Co., Ltd.
* Corresponding author. Key Laboratory for Ultrafine Materials of Ministry of Education, East China University of Science and Technology, Shanghai, 200237, PR China.
** Corresponding author. Engineering Research Center for Biomedical Materials of the Ministry of Education, East China University of Science and Technology, Shanghai, 200237, PR China..
*** Corresponding author. Frontiers Science Center for Materiobiology and Dynamic Chemistry, East China University of Science and Technology, Shanghai, 200237, PR China.
E-mail addresses: nanboshan1987@163.com (Z. Geng), biomatwj@163.com (J. Wang), liucs@ecust.edu.cn (C. Liu).

https://doi.org/10.1016/j.bioactmat.2021.05.003
Received 1 March 2021; Received in revised form 30 April 2021; Accepted 1 May 2021
Available online 12 May 2021

monocytes or macrophages, which primarily regulate the resorption of mineralized tissue or materials and play an important role in osseointegration [15,16]. Bone resorption caused by osteoclasts is coupled with osteogenesis of osteoblasts. After implantation, osteoclast-related bone resorption begins first around implants along with bleeding and inflammation. In specific, monocytes or macrophages migrate to the peri-implants and subsequently differentiate into osteoclasts in response to the stimulation of endogenous receptor activator of nuclear factor-κB ligand (RANKL) and macrophage colony stimulating factor (M-CSF) [17–19]. Osteoclasts then initiate bone resorption by releasing protons and enzymes [20]. Besides, osteoclasts are also associated with bone formation. Previous studies provided evidence that osteoclasts could resorb the bone matrix and further release active transforming growth factor-β1 (TGF-β1) to recruit MSCs and induce bone formation [21]. Pre-osteoclasts could also secrete platelet-derived growth factor-BB (PDGF-BB) to induce angiogenesis coupling with bone formation during bone metabolism [22]. Therefore, the function of osteoclasts should also be considered in promoting bone regeneration in bone defect.

Substantial efforts have been made in modifying the properties of scaffolds, which can regulate the fusion of osteoclasts. For example, recent studies showed the effect of topographical structure and crystallinity on osteoclast differentiation. Beta tricalcium phosphate (β-TCP) with sub-microstructure feature facilitated osteoclasts survival compared to that with microstructure [23]. Similarly, grain size of biphasic calcium phosphates (BCPs) was reported to affect the formation of multinucleated osteoclasts in dog ectopic model [24]. A recent study also showed that osteoclast could sense the crystallinity of materials and higher crystallinity promoted the resorption activity of osteoclasts [25]. Besides, surface roughness has also been shown to regulate osteoclast differentiation [24,26]. Furthermore, the impact of chemical composition on osteoclast behaviors has been studied in BCPs, and the results showed that the increase of hydroxyapatite (HA) content in BCPs decreased the number of bone marrow monocytes (BMMs)-derived osteoclasts [27]. Additionally, much attention has been paid to the ions released from materials as a strategy to modulate osteoclast behaviors [28–34]. Strontium-doped HA have been proved to strongly inhibit osteoclast differentiation owing to the incorporation of strontium ions. Besides, combining bioactive molecules by physically loading or chemically grafting with scaffolds has been proved as an effective strategy to regulate osteoclast behaviours [35–37]. Specifically, the study showed dicalcium phosphates bioceramic scaffolds coated with extra cellular matrix significantly reduced the generation of osteoclasts *in vivo* [36]. However, these studies mainly focused on inhibiting osteoclastogenesis, neglecting the coupling effect of osteoclast and osteoblast. Especially, the mechanism of how materials impacted the fusion of osteoclasts and the regulation of implant-induced osteoclasts on osseointegration balance between bone formation and bone resorption was rarely reported.

On the basis of these considerations, we strived to elucidate the effects of biomaterial on stimulating the osteoclast-mediated osseointegration. We selected CPC as the typical CaP, since it has been widely applied in clinic. To this end, we prepared a series of CPC scaffolds with different calcium and phosphate ratios (Ca/P), which was achieved by adjusting the amount of TECP and DCPA (Supplementary Table S1). We sought to illuminate the ionic effect of CPC on osteoclast behaviors. We found that phosphate ions released from CPC played the main role in modulating osteoclastogenesis. Excessive release of phosphate ions from low Ca/P ratio CPC significantly decreased osteoclastogenesis by the reduced affinity between RANKL and RANK, following by the inhibited expression of NF-κB signaling pathway. Slight release of phosphate ions from high Ca/P ratio CPC improved osteoclastogenesis via robust RANKL-RANK dependent NF-κB signaling pathway. Rat calvarial defect model further verified the ions effect on osteoclast-mediated osseointegration. Our findings might provide a new strategy for improvement of osseointegration.

2. Results

2.1. Ca/P ratio in CPC affected differentiation and function of osteoclasts

We first prepared different Ca/P ratio of CPC scaffolds (1.4CPC, 1.5CPC, and 1.67CPC) by altering the proportion of tetracalcium phosphate (TECP) and dicalcium phosphate anhydrous (DCPA). 1.67CPC possessed highest Ca/P ratio compared to other groups, and 1.4CPC possessed lowest Ca/P ratio. The final Ca/P ratio of CPC was listed as final Ca/P ratio (Supplementary Table S1) measured by ICP-OES after curing. Then, we detected the variation of phase composition of each CPC sample using X-ray diffraction (XRD) analysis (Fig. S1a). The peaks of three samples were all similar with typical HA patterns, indicating the main component of the samples was HA. Moreover, the crystalline peaks suggested Ca/P ratio in CPC presented negligible effect on the crystal structure of HA in CPC. All samples except for 1.67CPC had a typical DCPA peak, and the peak in 1.4CPC was more intense than that of 1.5CPC, indicating the excessive DCPA was left as shown in previous report [38]. In FT-IR spectrum, all samples had typical absorption peaks of phosphate and hydroxyl of HA. (Fig. S1b). The 1.4CPC group showed a more intense peak of phosphate at about 700 cm^{-1} than other groups.

To evaluate the effect of CPC on osteoclast differentiation, tartrate resistant acid phosphatase (TRAP) staining was performed. After 7 days of incubation with differentiation medium, we observed TRAP-positive osteoclasts on all CPC scaffolds, while more rigorously stained and largely interconnected osteoclasts were found on 1.67CPC group (Fig. 1a). Quantitative analysis (Fig. 1b) showed the number of TRAP-positive osteoclasts dramatically increased with the increase of Ca/P ratio, and the largest number of TRAP-positive osteoclasts were present on 1.67CPC group (nearly 340 in 1.67CPC group and only 160 in 1.4CPC group). The trends were confirmed by TRAP activity assay (Fig. 1c), in which the activity of osteoclasts in 1.67CPC group was significantly higher than other groups.

Next, we analyzed the morphology of osteoclast-like cells and their interaction with CPC scaffolds using scanning electronic microscope (SEM) (Fig. 1d). In 1.67CPC group, we found giant cells with numerous needle-like pseudopodia/filopodia (red arrow), which strongly demonstrated the typical osteoclast-like cell morphology and the oriented pseudopodia/filopodia extended to the surface of scaffolds indicating the close interaction between cells and materials. However, smaller cells with less pseudopodia/filopodia were found in 1.4CPC and 1.5CPC groups, which was also shown in the quantificaiton of pseudopodia/filopodia (Fig. 1f).

We further evaluated cell fusion, multinucleation, and formation of actin rings on CPC by fluorescence staining (Fig. 1e). We found much more intensely, massive multinucleated cells with fluorescent actin rings in 1.67CPC group compared to 1.4CPC and 1.5CPC groups, where multinucleated cells were smaller and sparsely distributed. During bone resorption, osteoclasts generate a circumferential “sealing zone”, where ruffled border (RB) is generated and exerts bone resorptive function [39]. As expected, we found more sealing zones (red arrow) in 1.67CPC groups compared to other groups (Fig. 1g), suggesting 1.67CPC group may promote the resorption ability of osteoclast.

Moreover, the resorption pits and inherent surface morphology of CPC were indistinguishable, which prompted us to apply indirect method to evaluate the resorption capability of the osteoclasts grown on CPC surface. As shown in Fig. 2a, we firstly incubated osteoclasts on CPC surface for 5 days, then, the cells were digested and reseeded on bone slice, after another 2 days of incubation, the bone slices were performed with TRAP staining (Fig. 2b, d) and resorption pits analysis (Fig. 2c, e, f). We found the differentiation trend of osteoclasts (Fig. 2b, d) on bone slices was consistent with that on CPC scaffolds (Fig. 1a and b). Compared to other groups, osteoclasts from 1.67CPC group were more intensely distributed on bone slice with clearly and larger boundaries. Furthermore, we discovered that 1.67CPC group showed much more resorption lacunae (white dash circle) on bone slices relative to other

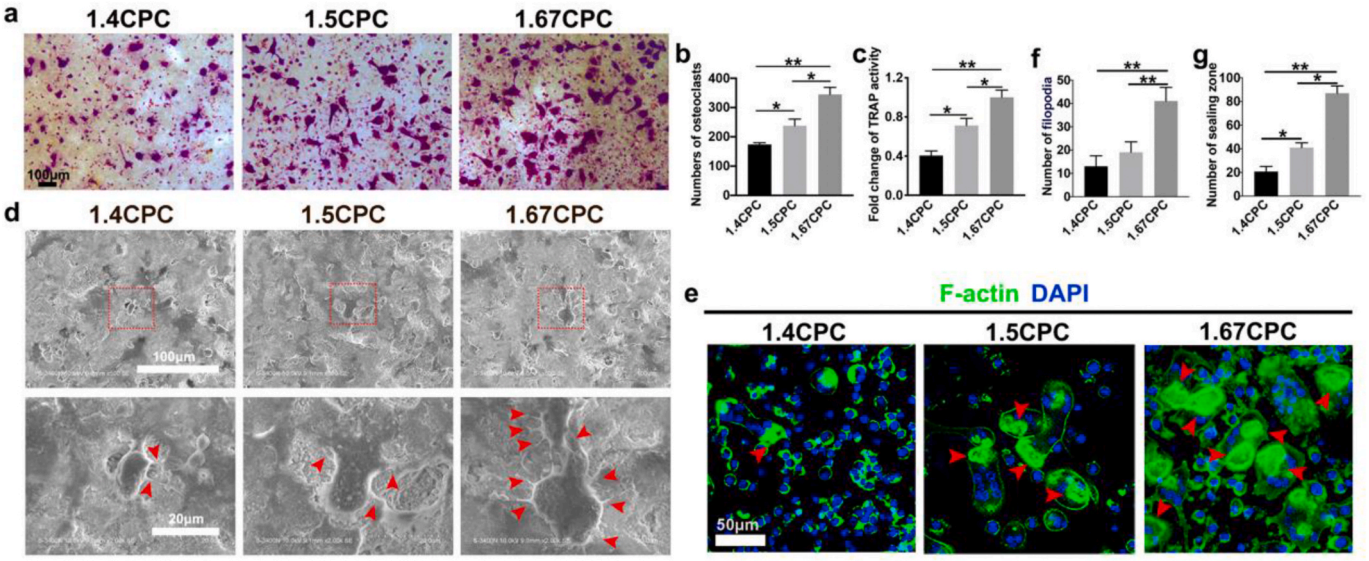

Fig. 1. The effect of various Ca/P ratio of CPCs on osteoclast differentiation. The experiments were conducted after culturing in differentiation medium for 7 days. (a) Representative images of TRAP staining (wine red). (b) Quantitative analysis of TRAP-positive osteoclasts (n = 4. For each sample, the number of osteoclasts in randomly six fields was added up and the size of field was the same as shown in Fig. 1a). (c) Quantification of TRAP activity (n = 4) normalized to 1.67CPC. (d) SEM images of osteoclasts on CPC surfaces, the red arrow presents the filopodia and quantification of filopodia was shown in (f) (n = 4. For each sample, the number of filopodia in randomly six osteoclasts was added up). (e) Representative confocal images of osteoclasts on surfaces of CPC scaffolds. The red arrow indicates the representative sealing zone of osteoclasts. (g) Quantification of sealing zone (n = 4. For each sample, the number of sealing zones in randomly six fields was added up and the size of field was the same as shown in Fig. 1e). (*P < 0.05, **P < 0.01).

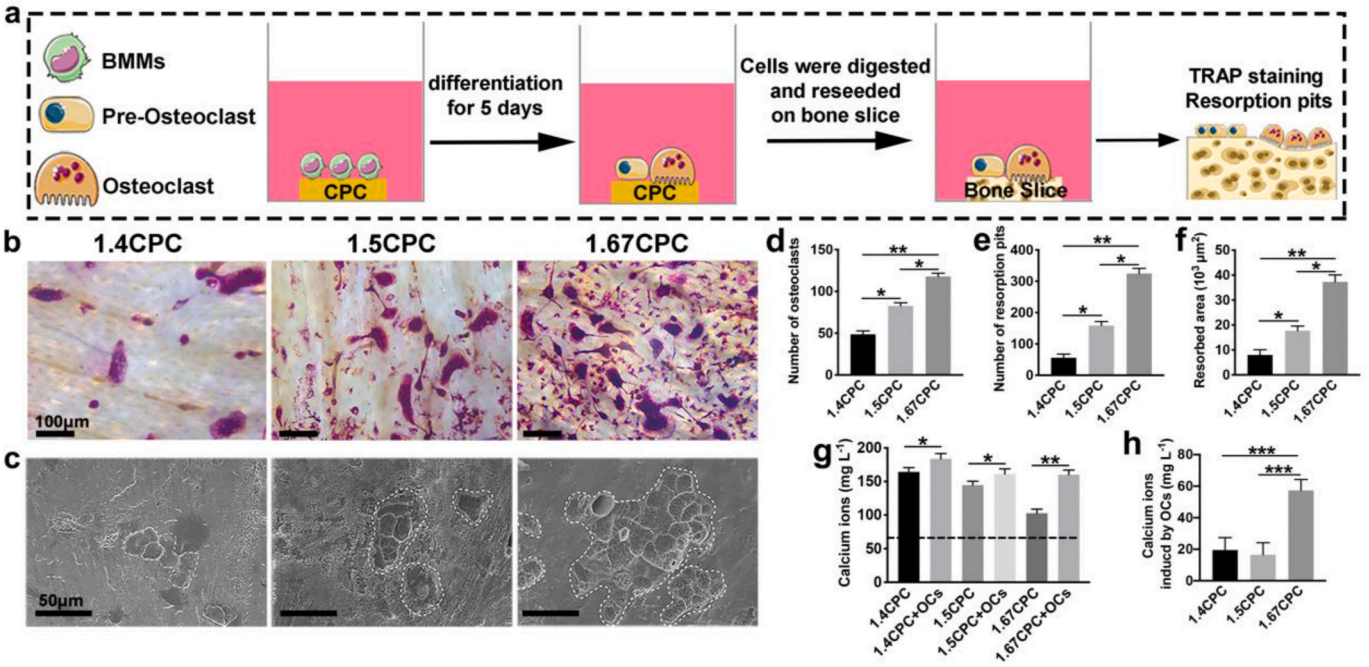

Fig. 2. The effect of various Ca/P ratio of CPCs on function of osteoclast. (a) The schematic of experimental procedures. (b) Representative TRAP-stained images on bone slices. (c) SEM results of resorption pits corroded by osteoclasts. (white dash lines indicate the boundaries of resorption area). (d) The number of osteoclasts on bone slice was counted (n = 4. For each sample, the number of osteoclasts in randomly six fields was added up and the size of field was the same as shown in Fig. 2b). (e) The number of resorption pits and (f) the resorbed area was counted (n = 4). (g) After 7 days of cultivation, the concentration of calcium ions in supernatant was measured by ICP-OES. Black dotted line represented the baseline level of calcium in culture medium (about 68 mg L^{-1}). (h) Calcium ions concentration induced by osteoclasts were quantified. Concentration of calcium ions induced by osteoclasts in each CPC group was acquired by subtracting calcium ions of CPC without osteoclasts from that with osteoclasts. (*P < 0.05, **P < 0.01, ***P < 0.001).

groups, where lacunae were smaller and sparsely distributed. Next, the number of resorption pits and the size of total resorption area were calculated (Fig. 2e and f), and the results showed that osteoclasts from 1.67CPC group could significantly enhance the resorption capability compared to 1.4CPC and 1.5CPC groups. At the end of incubation in transwell assay, the supernatant was collected for the measurement of TGF-β1, which could effectively recruit MSCs for osteogenesis [21]. The results (Fig. S3) showed that the concentration of TGF-β1 in 1.67CPC

group was significantly higher than other groups, which indicated that 1.67CPC could significantly promote TGF-β1-induced bone formation.

To further evaluate the bone resorption capability of osteoclasts on different CPC surface, we collected the supernatants after 7 days of incubation with differentiation medium, and the supernatant without BMMs were treated as control. Then, we measured the concentration of calcium ions in the supernatants using inductively coupled plasma optical emission spectroscopy (ICP-OES) (Fig. 2g). The results showed that each CPC group with osteoclasts had a higher concentration of calcium ions compared to the corresponding group without osteoclasts, which was because osteoclasts could resorb part of CPC and release calcium ions into medium. Calcium ions induced by osteoclasts were calculated by subtracting the calcium concentration without osteoclasts from that with osteoclasts. The results showed that 1.67CPC group had the highest concentration of calcium ions induced by osteoclasts among all groups (Fig. 2h), indicating that 1.67CPC group could significantly promote the osteoclast resorption capability relative to 1.4CPC and 1.5CPC groups.

2.2. Phosphate ions released from CPC played an important role in osteoclast differentiation

To explore the dominant factor resulting in the inhibition of osteoclast differentiation, we analyzed the surface topography of CPC sample using SEM (Fig. S2a-f). In 1.4CPC and 1.5CPC groups, some DCPA with plate-shaped crystals existed which was consistent with XRD results (Fig. S1a), while the surface of three CPC groups was mostly needle-shaped HA which was in line with XRD results (Fig. S1a). Besides, surface roughness analysis by atomic force microscope (AFM) demonstrated different Ca/P ratios in CPC have no effect on the average roughness (Ra) (Fig. S2g-j). Thus, we suggested that the morphology of CPC samples played a negligible role in osteoclast differentiation and function.

Next, we investigated the effects of ions released from CPC samples on osteoclastogenesis. Transwell assay was conducted as shown in the illustration (Fig. 3a). After 7 days of incubation with differentiation medium, we analyzed the resorption lacunae (Fig. 3b) and found that osteoclasts could resorb bone slices in all groups, and the variation trend of number of resorption pits was consistent with the abovementioned (Fig. 2c, e, f). The number of resorption pits in 1.67CPC group was significantly larger than that of 1.4CPC and 1.5CPC groups, while smaller than that of control group, and osteoclasts on 1.5CPC generated more resorption pits than that on 1.4CPC group (Fig. 3c). We found that the number of resorption pits and relative resorption area (Fig. 3d) increased as the Ca/P ratio in CPC increased from 1.4 to 1.67. Hence, we suggested that osteoclastogenesis and its resorption capability augmented in a Ca/P ratio-dependent manner.

The improved osteoclastogenesis on 1.67CPC surface enlightened us that the ions from CPC scaffolds may play the critical role in osteoclast differentiation. To confirm our assumption, we further measured the concentration of calcium ions (Fig. 3e) and phosphate ions (Fig. 3f) of CPC extract by ICP-OES. We found that the concentration of both calcium and phosphate ions in CPC extract decreased with the increasing

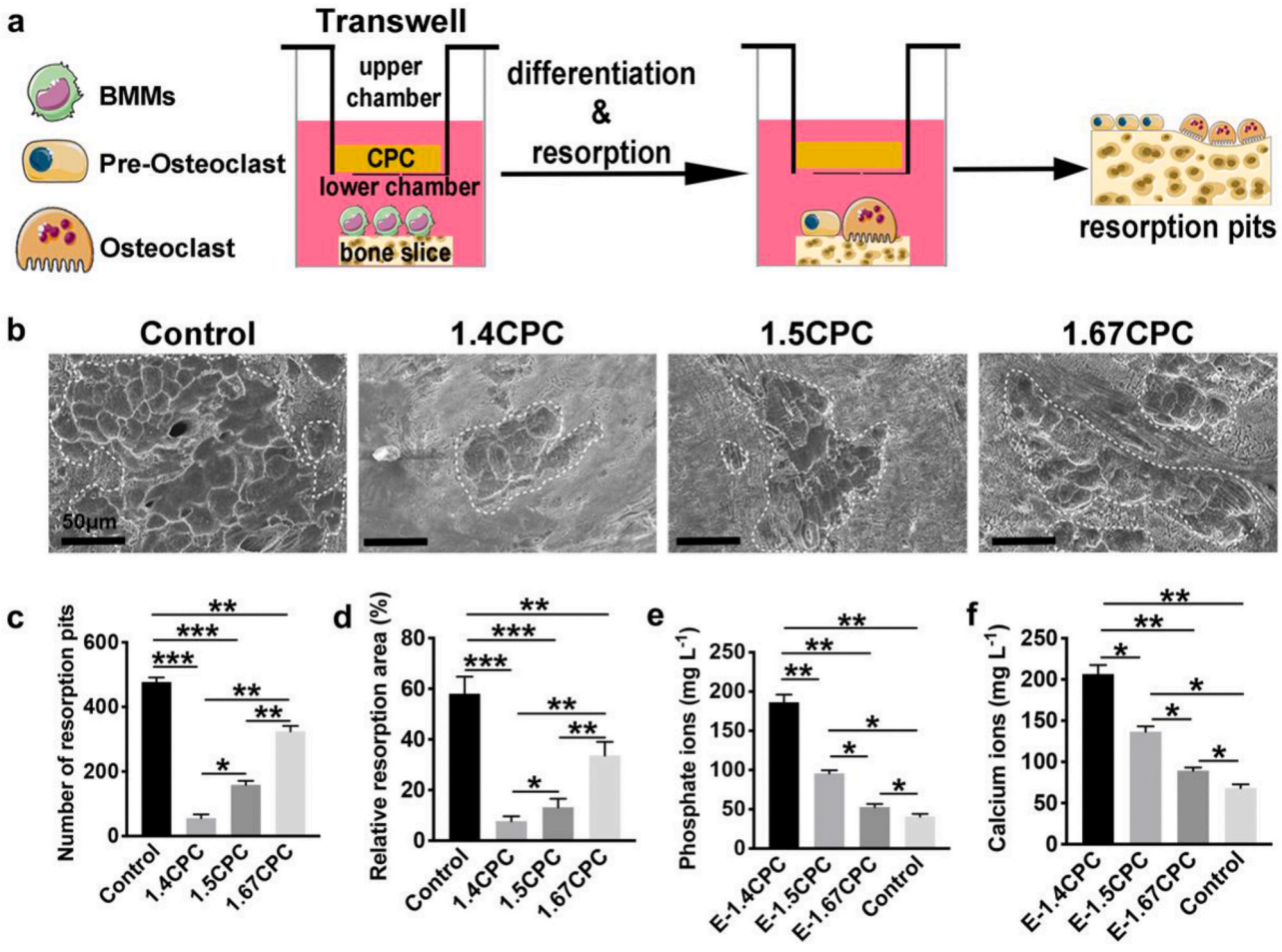

Fig. 3. The ions from CPC scaffolds played the main role in affecting osteoclast differentiation and function. (a) Schematic of transwell assays. (b) Resorption pits images of bone slice; the white dash lines mean the boundaries of corrosion area. (c) The number of resorption pits and (d) relative resorption area was counted. (e) The concentration of calcium ions measured by ICP-OES. (f) The concentration of phosphorous ions detected by ICP-OES. E-CPC indicated the extract of CPC samples. The culturing medium were regarded as control. (*$P < 0.05$, **$P < 0.01$, ***$P < 0.001$).

Ca/P ratio in CPC. Cell viability of BMMs was firstly evaluated with 3-(4,5-dimethylthiazol-2-yl)-2,5-diphenyltetrazolium bromide (MTT) assays after 3 days of incubation with CPC extracts. The results (Fig. S4) demonstrated no significant difference among three groups.

To further investigate the influence of CPC on osteoclastogenesis, we incubated BMMs with CPC extracts for 7 days and examined their effect on osteoclast differentiation. At the end of incubation, TRAP staining was performed (Fig. 4a). We found that all CPC groups had suppressive effect on osteoclast differentiation compared to the control group. However, 1.67CPC group had the largest number of osteoclasts and 1.4CPC had the minimum (Fig. 4b). We inspected the pH values of each CPC extract and the results showed that pH values of three groups ranged from 7.2 to 7.3, and no significant difference was observed (Fig. 4f), which indicated that pH values of CPC extracts had no significant effect on osteoclast differentiation.

Thus, after excluding the effect of pH value on osteoclast differentiation, we diluted CPC extract to further confirm the ion effect on osteoclast differentiation. 1.4CPC extract, which had the strongest inhibitory effect on osteoclastogenesis, was chosen as an example for further evaluation. We found that the number of osteoclasts was elevated with increased dilution times (3 times and 5 times), respectively reaching a 1.3-fold and 2.3-fold increase in the number of osteoclasts over that of initial 1.4CPC extract (Fig. 4c and d). The results indicated that osteoclast differentiation was inhibited by ions released from CPC samples in a concentration dependent manner.

Next, in order to figure out whether calcium or phosphate ions played a leading role in inhibiting osteoclast differentiation, osteoclasts were incubated with ethylene diamine tetraacetie acid (EDTA), a calcium chelator, in 1.4CPC extract differentiation medium. The number of osteoclasts in the EDTA-treated group was about 57, in contrast to 60 in non-treated group, which showed no significant difference. The results (Fig. 4e and Fig. S5a) indicated that calcium ions released from 1.4CPC sample had a negligible effect on osteoclastogenesis.

As previously mentioned, concentration of phosphate ions in each CPC extract was different, which was 200, 140, and 50 mg L^{-1} for 1.4CPC, 1.5CPC and 1.67CPC, respectively (Fig. 3e). Thus, we prepared differentiation medium containing various concentrations of phosphate ions (40, 90, 140, 190, 240, 440 mg L^{-1}) by adding extra phosphate ions (0, 50, 100, 150, 200, 400 mg L^{-1}) to investigate the effect of phosphate ions released from CPC samples on osteoclastogenesis. The results depicted an obvious trend that with the increasing concentration of phosphate ions in medium, the number of osteoclasts decreased gradually (Fig. 4g and Fig. S4b), which was consistent with our previous results (Fig. 4b). Taken together, these results indicated that phosphate ions released from CPC samples, instead of calcium ions or pH value, played the leading role in inhibiting osteoclast differentiation.

2.3. High Ca/P ratio of CPC induced OCs differentiation via RANKL-RANK signaling

The mechanism whereby phosphate ions released from CPC scaffolds inhibit osteoclast differentiation was then investigated. We detected the expression level of RANK in osteoclasts after 7 days of incubation on CPC samples by confocal laser scanning microscope (CLSM) (Fig. 5a). Compared to 1.4CPC and 1.5CPC groups, more red fluorescence of RANK was observed when osteoclasts were incubated on 1.67CPC group (Fig. 1e), reflecting that RANK expression was obviously improved by 1.67CPC. Enzyme linked immune sorbent assay (ELISA) assays further

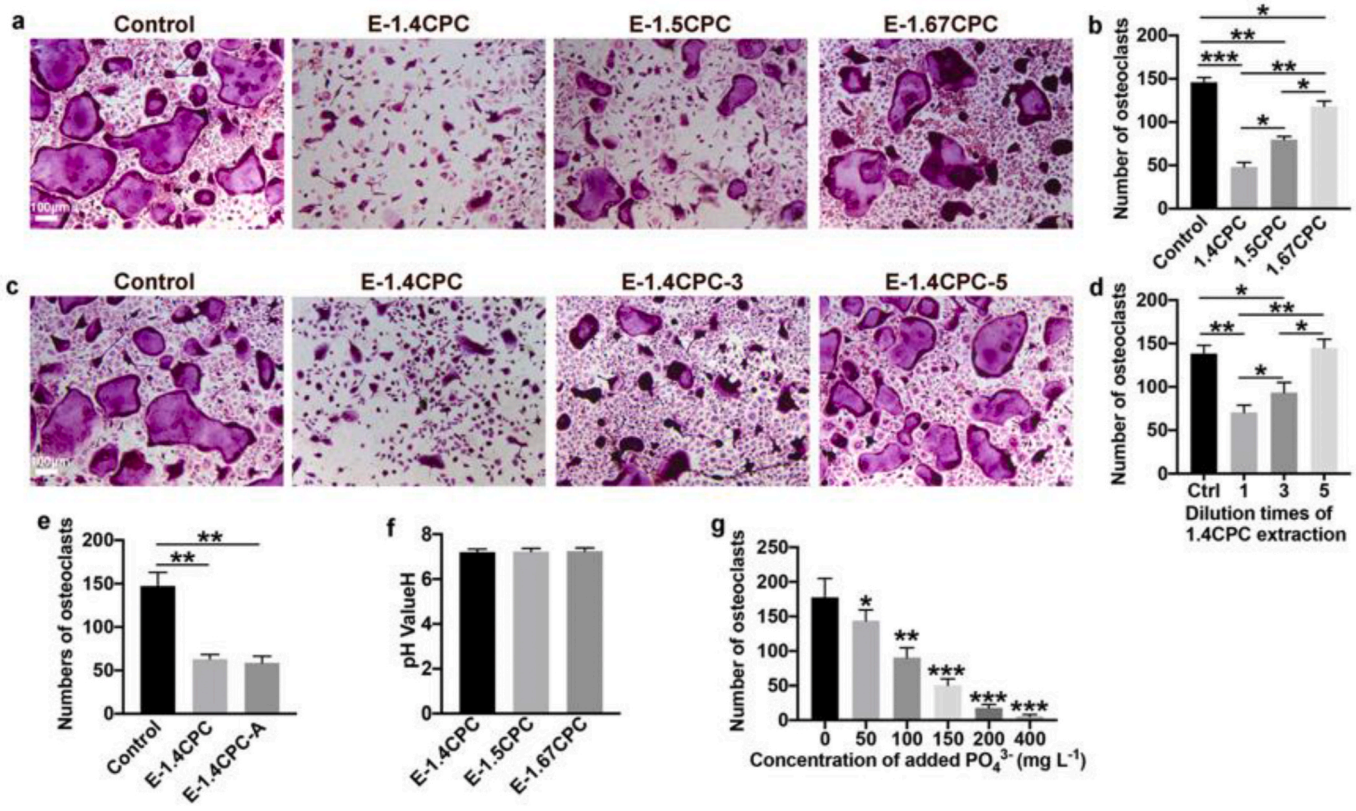

Fig. 4. Phosphate ions released from CPC scaffolds inhibited osteoclast differentiation. CPC extracts were used to further investigate the ions effect on osteoclast differentiation released from the CPC scaffold. BMMs were cultured with M-CSF and RANKL in extract medium for 7 days, subsequently with TRAP staining. (a) The images of TRAP-positive osteoclasts and (b) the number of osteoclasts were counted. (c) TRAP staining images, E−1.4CPC-3 and E−1.4CPC-5 represent 3 times dilution and 5 times dilution of 1.4CPC extract, respectively. The untreated medium was used as diluent. (d) The number of osteoclasts were quantified. (e) The number of osteoclasts were counted. E−1.4CPC-A means the 1.4CPC extract was treated with EDTA. (f) The pH value of CPC extracts. (g) The number of osteoclasts were counted after cultivating BMMs with different concentration of phosphate ions. (*$P < 0.05$, **$P < 0.01$,***$P < 0.001$).

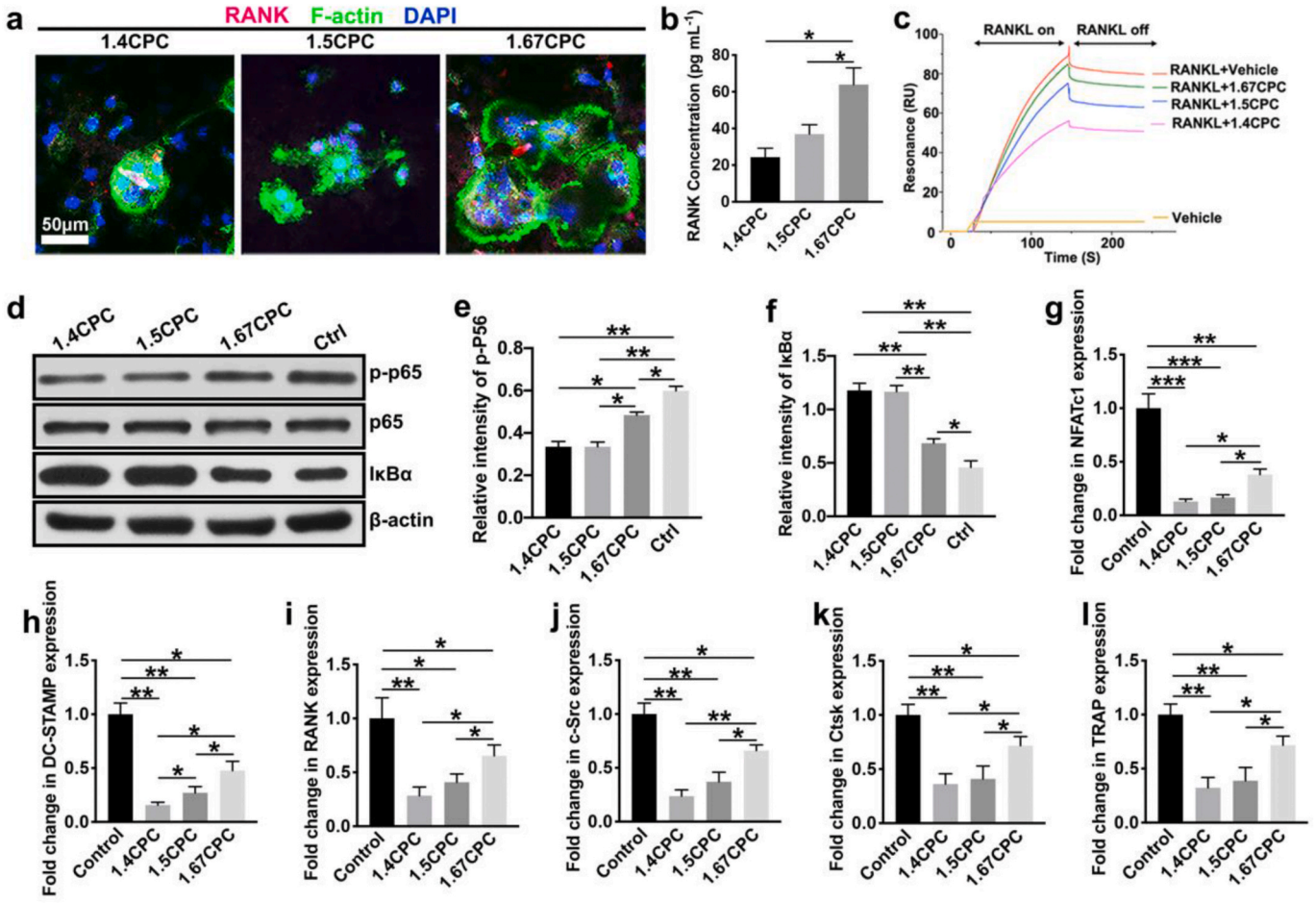

Fig. 5. Effect of Ca/P ratio in CPC on RANKL-RANK signaling. (a) Immunofluorescence analysis of RANK expression (red) in osteoclasts on surface of CPC scaffold. (b) Concentration of RANK was analysis by ELISA. The concentration of RANK was measured after inducing BMMs for 1 days. (c) Affinity between RANKL and RANK was measured in BIAcore T200 system. Human-RANK anchored on the chip was applied to interact with the human-RANKL dissolved into the CPC extract. The vehicle means MEM-α medium. (d) 1.67CPC promoted RANKL-induced phosphorylation of NF-κB p65, and degradation of IκBα. (e) p-p65 and (f) IκBα intensity of Western blot bands was calculated with normalizing to β-actin. The untreated medium was treated as control. (g–l) Relative mRNA expression of osteoclast was measured after inducing BMMs for 7 days in CPC extract. BMMs cultured with untreated medium was treated as control. (*P < 0.05, **P < 0.01,***P < 0.001).

validated that the expression level of RANK was significantly elevated in 1.67CPC group after 1 day of incubation (Fig. 5b). The results suggested that 1.67CPC significantly enhanced RANK expression level of osteoclasts.

Previous studies demonstrated that the increased affinity of RANKL for RANK can generate more robust downstream signaling and has stronger osteoclastogenic potential in osteoclast-lineage cells [40]. We then evaluated the affinity of RANKL for RNAK in CPC extracts by surface plasmon resonance (SPR) analysis (Fig. 5c). The results showed that 1.67CPC group which possessed minimum phosphate ions had the highest RU (resonance units) level which represents the intensity of affinity, relative to 1.4CPC and 1.5CPC groups, which indicated that excessive phosphate ions from CPC scaffolds decreased the affinity of RANKL for RANK. Next, we examined the expression of NF-κB signaling pathway, which is the downstream mediator of RANK and strongly associated with osteoclast differentiation. The visualization of protein bands and quantitative analysis showed that RANKL-induced phosphorylation of NF-κB p65 was remarkably up-regulated, whereas the expression of IκBα was significantly down-regulated in 1.67CPC group relative to 1.4CPC and 1.5CPC groups. The down-regulated expression of IκBα means 1.67CPC promoted the degradation of IκBα and facilitated the transduction of NF-κB signaling. Thus, these results demonstrated that NF-κB signaling induced in 1.67CPC group was more robust than that of 1.4CPC and 1.5CPC groups.

Next, osteoclast-related gene expressions in osteoclasts stimulated by CPC extracts was examined by real time fluorescent quantitative reverse transcription polymerase chain reaction (qRT-PCR). Relative mRNA expressions of c-Src, NFATc1, DC-STAMP, RANK, TRAP and Cathepsin K (Ctsk) were evaluated after incubating BMMs with CPC extracts for 7 days. The results showed both osteoclastogenesis-related genes (c-*Src, Nfatc1, Dc-Stamp, and Rank*) (Fig. 5g–j) and functionalized genes (*Trap and Ctsk*) (Fig. 5k and l) were up-regulated with the increased ratio of Ca/P in CPC. These results were consistent with SPR and Western blot results, further indicating that CPC of high Ca/P ratio could significantly promote osteoclast differentiation.

2.4. *High Ca/P ratio CPC promoted the osseointegration of bone defect in vivo*

We next evaluated the capacity of bone regeneration in a bilateral rat calvarial defect model with implanted porous CPC scaffolds of different Ca/P ratios. We firstly measured the porosity of porous CPC scaffolds as previously described [8]. The results showed that no significant difference was found among three groups with the average porosity of 70% (Fig. S6). The *in vivo* results showed that 1.67CPC group had a better bonding interface relative to other groups, whereas 1.4CPC group possessed a bigger gap between host bone and implant (Fig. 6a, f), reflecting that high ratio of Ca/P in CPC promoted bone healing.

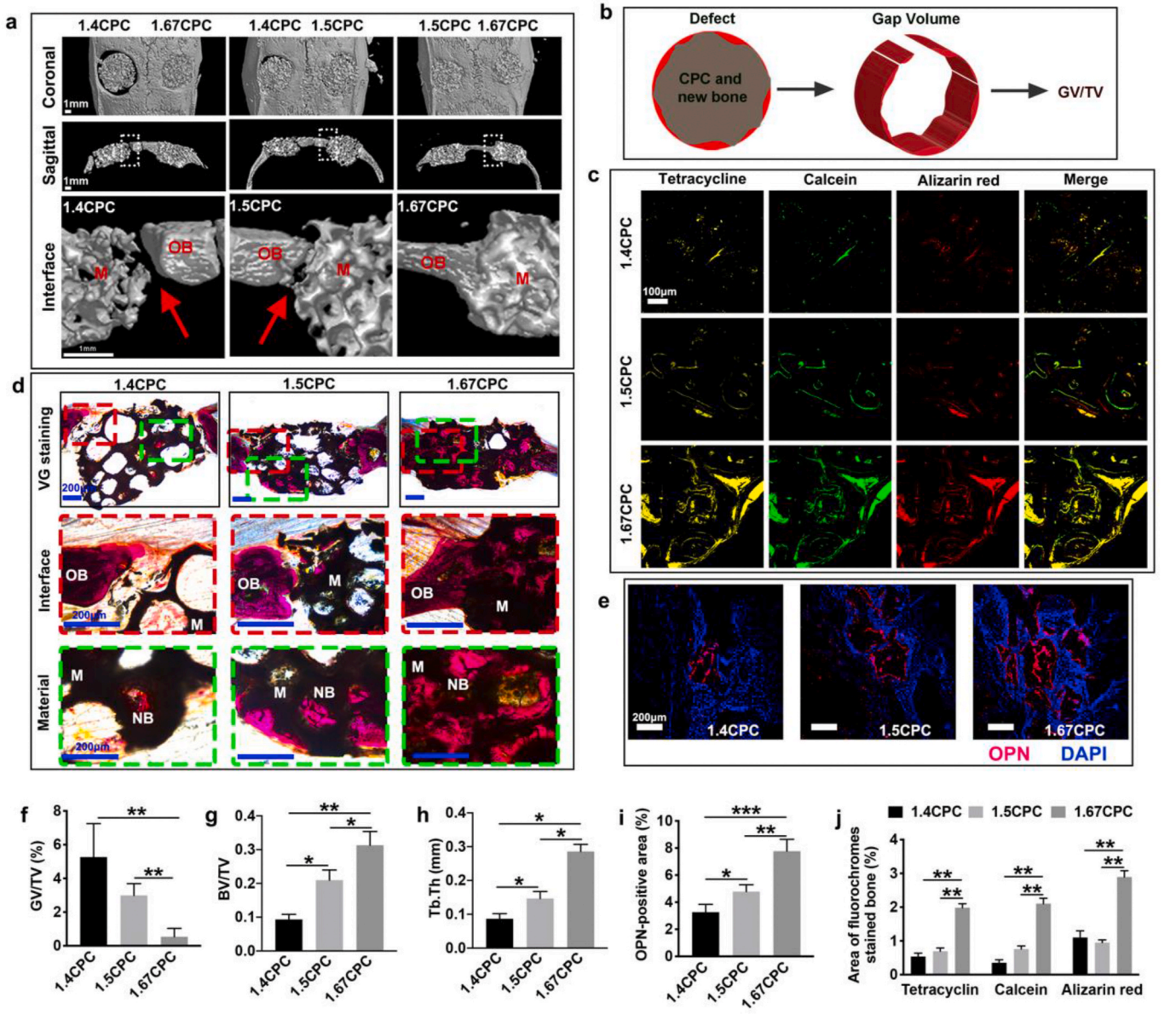

Fig. 6. 1.67CPC accelerated the osseointegration in a calvarial defect of SD rats. (a) The images of 3D reconstruction demonstrated the remediation effect of different CPC scaffolds. The white dashed box represented the interface between the material (M) and the old bone (OB). The bottom images represented the magnified area of the white dash box. (b) The schematic of definition of GV/TV. GV and TV indicated gap volume between host bone and implant and tissue volume, respectively. The gap volume was acquired by the unrepaired volume divided by whole defect volume. (c) Determination of new bone generation and mineralization by fluorescence-labeling analysis. Color in yellow represented tetracycline at week 3, green represented calcein at week 6, red represented alizarin red at week 9, and the merged represented the combination of the three fluorescence-labeling images. (d) VG staining Images of new bone formation in calvarial defects. The red dash box means the interface between the material and the old bone, and the green one means the material area. (e) Immunofluorescent staining of OPN after 12-week operation. (f) The gap volume/total volume (GV/TV). (g) Bone volume/total volume (BV/TV). (h) Trabecular thickness (Tb. Th). (i) The proportion of OPN positive region in the view field. (j) The percentage area of fluorescence-labeling newly formed bone in different CPC groups. (*P < 0.05, **P < 0.01, ***P < 0.001).

Additionally, compared to 1.4CPC and 1.5CPC groups, 1.67CPC group entailed significant increases in bone volume (BV/TV) and thickness of trabecular (Tb. Th) (Fig. 6g, h) and a obvious decrease in gap volume (GV/TV) (Fig. 6b, f). Moreover, we assessed the effect of different groups on new bone formation and mineralization during bone defect healing. Sequential fluorescence labeling, tetracycline (yellow), calcein (green), and alizarin red (red), was respectively performed at 3, 6, and 9 weeks post-operation to assess bone healing capability of CPC at early and late stage of bone healing, and the data were recorded by CLSM and analyzed by Image Pro Plus (version 5.0) (Fig. 6c). The fluorescence-labeled staining showed that 1.67CPC group possessed the largest fluorescent area compared to other groups at week 3, 6, and 9, respectively. Van Gieson (VG) staining was performed to assess new bone formation and osseointegration. The representative VG staining images showed that 1.67CPC group exhibited more new bone formation relative to other groups in the regions of interest, which was consistent with the GV/TV results (Fig. 6a, d, f). Especially, the newly formed bone in periphery of 1.67CPC group was totally connected with the host bone without macroscopic crevice and exhibited an excellent property of osseointegration. Taken together, the results delivered the following order of osseointegration performance of CPC scaffolds: 1.67CPC > 1.5CPC > 1.4CPC.

We also utilized osteopontine (OPN) staining to explore the osteogenic effect of CPC scaffolds with different Ca/P ratios in bone defect

healing (Fig. 6e, i). During osteogenic differentiation, OPN secreted from MSCs would be greatly upregulated [41–44]. We found 1.67CPC group exhibited the largest red area relative to other groups, demonstrating that 1.67CPC remarkably enhanced OPN-related osteogenesis. Hence, 1.67CPC group significantly improved the capability of new bone formation and osseointegration in bone defect repair.

Besides, we evaluated the ability of osteoclast differentiation of different CPC groups in bone defect model via TRAP staining (Fig. 7a and b). It could be observed that all groups possessed TRAP-positive osteoclasts, whereas more osteoclasts were observed in 1.67CPC group relative to other groups. Notably, more osteoclasts were found on material area in 1.67CPC group, indicating that 1.67CPC could provide a better micro-environment for osteoclastogenesis as well as bone remodeling relative to other groups. Additionally, we measured the expression level of TGF-β1 activated by osteoclasts which can recruit MSCs to the resorption site for new bone formation (Fig. 7c) [21,22]. Compared to 1.4CPC and 1.5CPC groups, 1.67CPC group generated much more TGF-β1 which was consistent with our previous findings that 1.67CPC group significantly promoted osteoclasotogenesis (Fig. 7a and b). Thus, 1.67CPC could significantly promote osteoclast differentiation and effectively enhance the expression level of TGF-β1 compared to other groups.

3. Discussion

Osseointegration in bone regeneration is crucial in preventing implant failure and strengthening its function [45–47]. Previous studies have shown improved *in vitro* bioactivity of scaffolds can enhance osseointegration [45]. Accumulated evidence focuses on MSC-mediated osteogenesis by upgrading its capacity of recruitment and proliferation [5–8], and these studies associated with osteoclast behaviors *in vivo* often hold the idea that osteoclasts are detrimental to bone osseointegration and should be inhibited [30]. However, the role of osteoclast involved in osteoclast-mediated osteogenesis and further osseointegration is neglected. Here, we found CPC samples with various Ca/P ratio could regulate osseointegration by altering osteoclastogenesis. Especially, high Ca/P ratio CPC scaffolds (i.e., 1.67CPC) significantly promoted bone healing through enhancing osteoclastogenesis along with robust secretion of TGF-β1.

Previous studies suggested that the released ions from CaP also affected the fusion of osteoclasts [48]. Here, we showed that the released calcium ions from various CPCs exhibited a negligible effect on

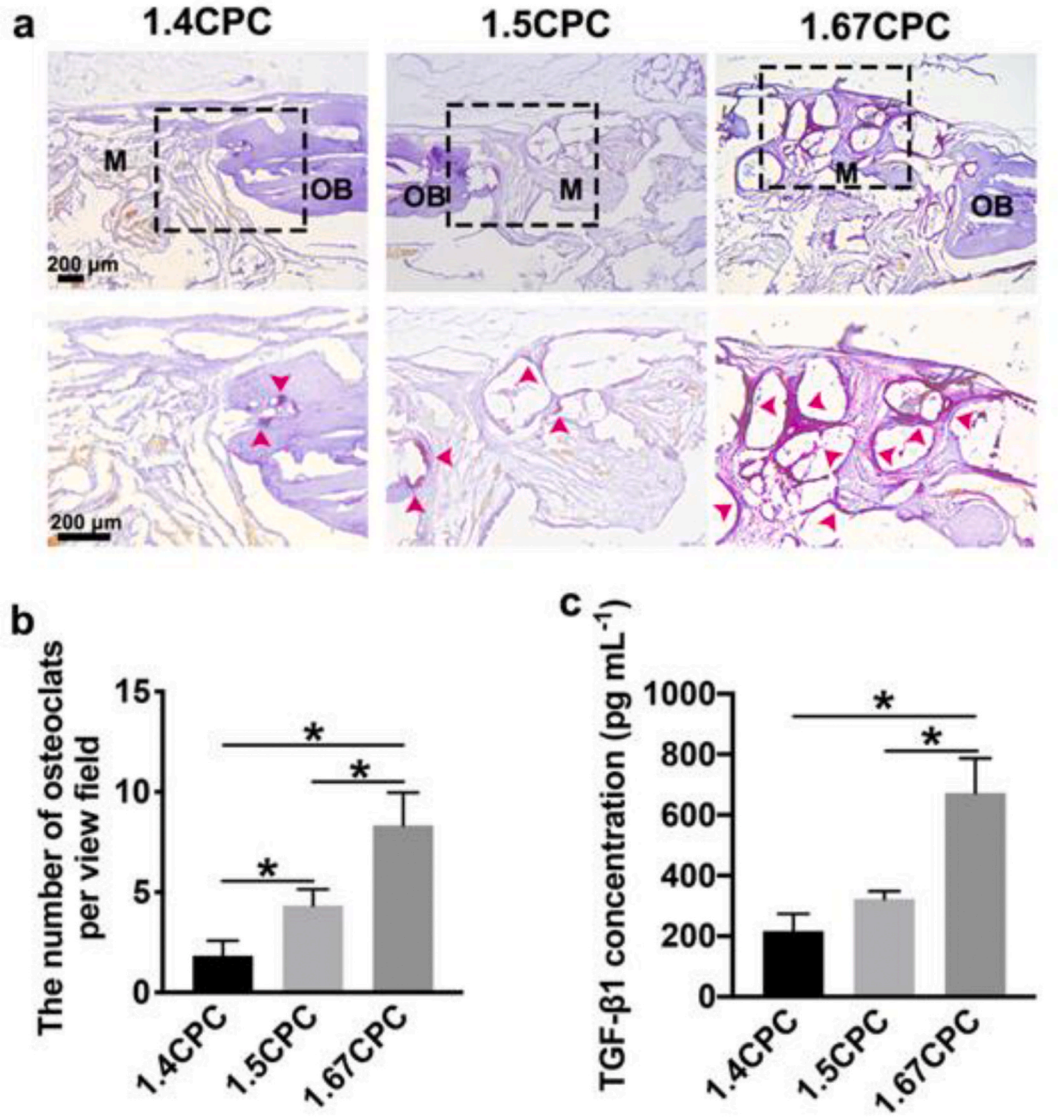

Fig. 7. 1.67CPCs promoted the osteoclastogenesis *in vivo*. (a) Images of TRAP staining. (b) The numbers of osteoclasts per view field was counted. (c) The concentration of TGF-β1 measured by ELISA at bone defect after implantation of different CPC samples at week 12. (*$P < 0.05$).

RANKL-induced osteoclastogenesis. Given that the inhibitory concentration of extracellular calcium ions on osteoclasts was extremely high (about 10 mM) [49], which was higher than released calcium ions from CPCs (4 mM at most), we anticipated that the released calcium ions were not involved in osteoclastogenesis in this study. Additionally, abundant evidence indicated that excessive phosphate ions could inhibit osteoclast behaviors [50]. We also confirmed the inhibitory effect of phosphate ions on osteoclasts by a series of experiments (Fig. S5b and Fig. 4g). The phosphate ions released from CPC samples significantly affected the RANKL-induced osteoclastogenesis, which was verified by dilution assays of phosphate ions (Fig. 4c and d). It has been reported that salt bridges in proteins are bonds between residues with opposite charges that are close enough to each other to generate electrostatic attraction, which are significantly important contributors to the structure and function of proteins [51]. In addition, glutamic acid and aspartic acid of RANK can form salt bridges with lysine and arginine of RANKL, respectively [52]. By this token, we speculated excessive phosphate ions released from CPC scaffolds may interfere electrostatic attraction between RANKL and RANK, hindering the formation of salt bridges between RANKL and RANK, and detrimentally affect the binding of RANKL and RANK with an inhibition of the phosphorylation of the downstream signaling. Thus, regulating the release kinetics of phosphate ions from CaP can effectively mediate osteoclast activity and bone integration. Additionally, it has been reported that chemistry/phase composition and surface roughness were important factors in regulation of cell responses [24,53]. Few chemistry/phase composition of DCPA existed in 1.4CPC and 1.5CPC groups as shown in results of XRD (Fig. S1a) and SEM (Fig. S2a-f), which was consistent with previous study [38]. However, no significant difference of surface roughness was found among three groups observed by AFM (Fig. S2g-j), indicating minor variation of DCPA did not lead to the difference of surface roughness. Thus, we suggested that the surface appearance of CPC samples was not the main role in regulating osteoclast differentiation. In addition, DCPA was mainly dissolved in alkaline solution [54], while, in this study, CPC samples were mostly in neutral solution where DCPA was hardly dissolved, which indicated that the ions released from CPC sample may not be derived from DCPA phase. Taken together, DCPA phase had a negligible effect on osteoclast differentiation in terms of ionic dissolution or surface topography. In addition, our results were consistent with the mechanism proposed by Bohner et al. [55] that low concentration of phosphate/calcium ions in tissue would facilitate heterotopic ossification.

It is well-acknowledged that RANKL is an exclusive ligand that binds to the extracellular domain of RANK [17]. The process of osteoclastogenesis is dramatically affected by the RANKL-RANK signaling pathway, and the RANKL-induced RANK internalization is indispensable for transduction of down-stream signaling like NF-κB and is necessary for inducing osteoclast formation and function [21,56,57]. In this study, we found that CPC with high Ca/P ratio obviously promoted the binding efficiency between RANKL and RANK in SPR assay (Fig. 5c) and promoted the expression of RANK on cell membranes (Fig. 5a and b). As compared, the CPC with lower Ca/P ratio incrementally hindered the RANKL-induced NF-κB signaling pathway and then negatively regulated the osteoclastogenesis (Fig. 5d–f). Besides, qRT-PCR analysis also confirmed that CPC groups with high Ca/P ratio significantly up-regulated osteoclast-related genes (e.g., *Nfatc1*, *Dc-Stamp*, *c-Sre*, *Ctsk*, and *Trap*) (Fig. 5g-l), which might result from more robust NF-κB signaling relative to the CPC groups with low Ca/P ratio.

At the stage of resorption, osteoclasts generate a sealing zone between cells and the surface of bone or apatite-based substrate, and inorganic substrates are dissolved by acidification of released protons, together with the organic component degradation by enzymes such as TRAP and Cathepsin K [20,58]. Here, we found more sealing zones were generated on surface of CPC with high Ca/P ratio, indicating more resorption sites were produced by osteoclasts relative to other groups (Fig. 1e). And the results of calcium ions induced by osteoclasts also verified that CPC with high Ca/P ratio could provide a more suitable microenvironment for osteoclast resorption compared to CPC with low Ca/P ratio (Fig. 2h).

The process of osseointegration always involves various factors, such as host cells, implants, and cytokines, which participates jointly in bone remodeling [29,59]. Osteoclasts perform a vital role in osseointegration with an activation by cytokines at implant interface, whereas any inhibition in osteoclastogenesis may retard bone healing [60,61]. Here, we observed that CPC with high Ca/P ratio exhibited an excellent property of osseointegration with a significant induction of osteoclasts which was consistent with our *in vitro* results. As compared, low Ca/P ratio group showed obvious inhibition of osteoclast fusion, whereas it was not conducive to osseointegration (Figs. 6 and 7). Since activated osteoclasts could resorb bone matrix and release endogenous TGF-β1 to recruit MSCs and induce osteogenesis [21,22], osseointegration could be regulated by CaP. The over quick dissociation in CPC with low Ca/P ratio was not consistent with moderated osteogenesis, which might also result in its poor osseointegration.

Our results revealed that CPC scaffold with high Ca/P ratio (i.e., 1.67CPC) profoundly promoted osteoclastogenesis and resorption capability along with an elevated secretion of TGF-β1, and finally upgraded the osseointegration in bone defect. As compared, overdose of released phosphate ions from CPC scaffold with low Ca/P ratio (i.e., 1.4CPC) significantly suppressed the binding of RANKL and RANK, and subsequently prevented the expression of RANK and its downstream signaling pathway (Fig. 8). Thus, the osteoclastogenesis in CaP was mediated by phosphate ions in a concentration-dependent manner through NF-κB signaling pathway. Besides, we found that CaP directly participated in bone healing through mediating osteoclastogenesis by released ions. The tunable property for osteoclastogenesis by regulating Ca/P ratio in CPC may be used in over-activated osteoclastogenesis situation such as osteoporosis.

4. Conclusion

In conclusion, this study provides insight into the capacity of CaP to effectively regulate osteoclast differentiation, and further facilitate osteoclast-mediated osseointegration. Besides, we provide evidence that overdose of phosphate ions released from CaP have negative effect on osteoclastogenesis by suppressing RANKL-RANK binding. CPCs with high Ca/P ratio can promote the osteoclast differentiation through NF-κB signaling pathway. Additionally, the *in vivo* experiment data support that CaP ameliorate osseointegration in high Ca/P ratio. Our results highlight the importance of not only deepening our understanding of traditional CaP, but also providing new strategy to promote bone repair.

5. Experimental section

5.1. Fabrication of CPC

The CPC scaffolds were fabricated by hydration reaction as previously reported [62]. The procedures were as follows: powders of TECP ($Ca_4(PO_4)_2O$, Shanghai Rebone, China) and DCPA ($CaHPO_4$ Shanghai Rebone, China), were mixed at a specific ratio (Supplementary Table S1), referred to 1.4CPC, 1.5CPC, and 1.67CPC, respectively, according to atomic ratio of calcium to phosphate. In the mixing process, 100 μL purified water was incorporated to form cement slurry. The slurry was cast into the mold under the pressure of 2 MPa for 1min to fabricate cylinder samples (Φ5 x 2 mm for *in vivo* experiments). The samples were cured for 3 days in the condition of 100% air humidity and 37 °C, after which, the samples were immersed into purified water for 3 days (change water every 6 h) and then dried at 37 °C for 24 h to obtain the CPC tablets.

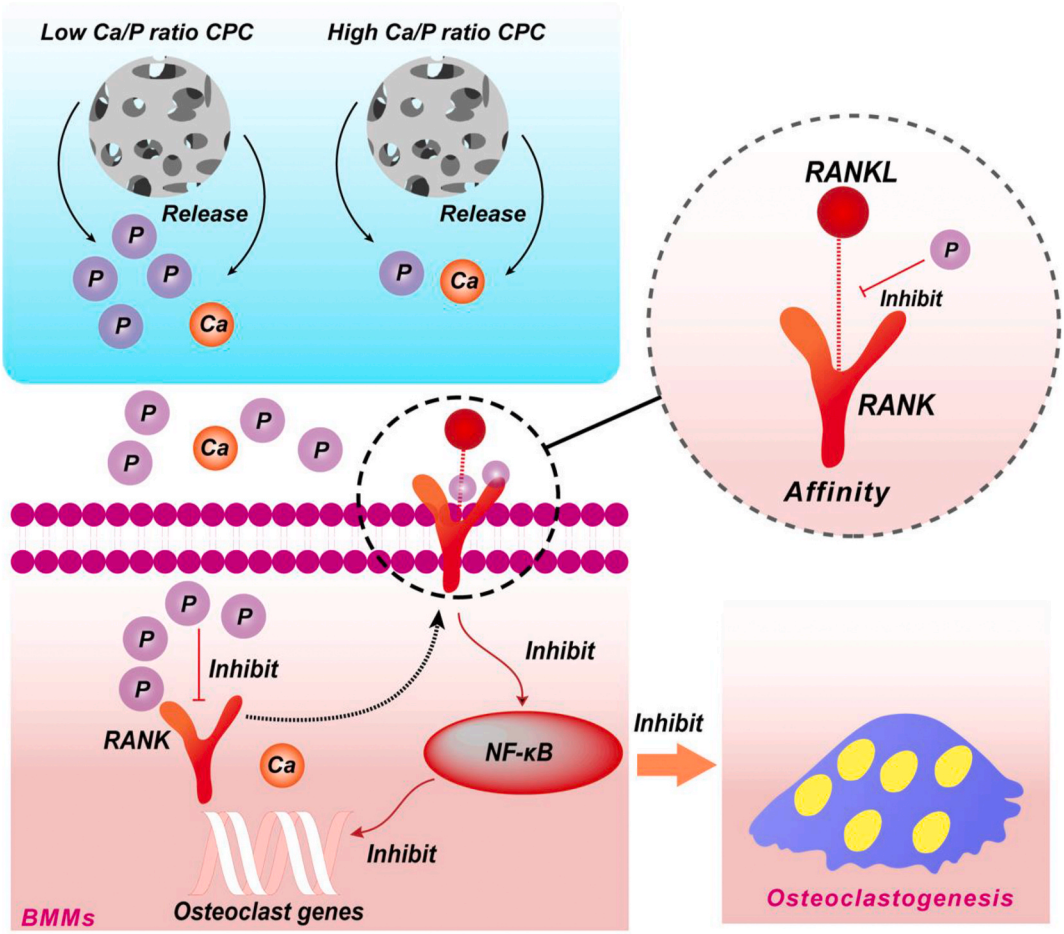

Fig. 8. Illustration of phosphate ions released from CPC scaffolds modulate osteoclastogenesis. Phosphate ions released from CPC scaffolds could significantly decrease the RANK expression; simultaneously inhibit the affinity between RANKL and RANK, thereby impeding the signaling cascades and down-regulating osteoclast targeted genes, which finally inhibited the osteoclast differentiation.

5.2. Preparation of CPC extracts

CPC extracts were prepared by soaking the CPC tablets in serum-free α-MEM medium at a surface area/volume ratio of 3 cm^2 mL^{-1} for 24 h at 37 °C. The pH values of the CPC extracts were measured through a pH meter (FE28, Mettler Toledo, Switzerland). CPC extract dilution assays were performed as follows: 1.4CPC extract was diluted 3 times and 5 times respectively with serum-free α-MEM medium for the further experiment. Calcium chelating method was applied to examine the effect of calcium ions on osteoclast differentiation. EDTA, which can effectively chelate divalent ion, was added into 1.4CPC extract at a final concentration of 1 mM to chelate free calcium ions in medium for further experiments.

5.3. Chemicophysical characterization

Chemical phase composition of CPC with different Ca/P ratios, was characterized using XRD (Rigaku D/max 2550VB/PC, Japan) in a continuous scan mode (2θ ranged from 10° to 80°), with Cu K α radiation (λ = 0.154 nm, 450 mA, 40 kV). Chemical structures of CPC samples were analyzed by fourier transform infrared (FT-IR, Nicolet, 5700, Thermo, USA) via KBr press-disk method, and the spectra were recorded over the range of 400–4000 cm^{-1}. Surface morphology of CPC samples was characterized by SEM (S-4800, Hitachi, Japan). The CPC tablets were treated in ascending concentrations of ethanol (70%, 80%, 90%, 95%, and 100%) for 20min at each gradient, with absolute ethanol employed twice. Then, the samples were vacuum-dried for 2 h at 37 °C. Subsequently, the samples were observed by SEM. Surface roughness of CPC tablets was measured by AFM (SPM-9700, Japan). In this study, the concentration of calcium ions and phosphate ions was measured by ICP-OES (Agilent 725, USA).

5.4. Osteoclast culture

For osteoclast differentiation assays, bone marrow monocytes (BMMs) were isolated from 6-week-old wild-type C57/BL6 male mouse (Shanghai jiesijie experimental animal Co., Ltd, China) femur and tibia bones [15]. Firstly, CPC tablets and bone slices were immersed into α-MEM medium (Thermo Fisher Scientific, USA) for 4 h at 37 °C, and then BMMs were seeded (5×10^4 per mm^2) respectively on CPC tablets, bone slices (Immunodiagnostic Systems Limited, UK) and cell culture plates (Corning, USA). α-MEM medium with 10% fetal bovine serum (FBS, Thermo Fisher Scientific, USA), 10 ng mL^{-1} M-CSF (R&D. USA) and 100 ng mL^{-1} RANKL (R&D. USA), was referred to differentiation medium. BMMs were then incubated for 7 days with differentiation medium (differentiation medium was replaced every 2 days) to investigate the differentiation and function of osteoclasts.

MTT assays was conducted to detect the cell viability in different CPC extracts. Briefly, BMMs were incubated with different CPC extracts containing M-CSF for 3 days. After that, medium with MTT was added into cell plates for another 4 h of incubation. At the end of experiment, the resulting solution was measured in cell plate (spectra MAX M2, Molecular Devices, USA) to record the optical density (OD).

CPC tablets were divided into two groups with or without BMMs

seeded on them for evaluation of osteoclast function. The supernatants were respectively collected to measure the concentration of calcium and phosphate ions. The concentration of calcium ions of CPC tablets with osteoclasts minus that of corresponding CPC group without cells was regarded as the concentration of calcium ions resorbed by osteoclasts. In data (Fig. 2g), The "CPC + OCs" means the osteoclasts were cultivated on CPC surface, and the "CPC" means CPC samples were soaked in culturing medium without osteoclasts.

5.5. Osteoclast differentiation in phosphate ions-added medium

Monosodium Phosphate (NaH_2PO_4, Sigma-Aldrich, USA) was used as the source of phosphate ion and added into medium with the final phosphate ion concentration of 40, 90, 140, 190, 240, and 440 mg mL^{-1}, respectively. The prepared differentiation medium was then utilized for osteoclast differentiation followed by TRAP staining.

5.6. TRAP staining assays

TRAP, a typical osteoclast marker, was utilized to characterize the differentiated osteoclasts. Briefly, the cells on samples were fixed with 4% paraformaldehyde for 1 h at room temperature, followed by staining with a commercial TRAP staining kit (387 A, Sigma, USA) according to the manufacturer's instructions. The images of TRAP staining were collected by inverted microscope (DMi8, Leica, Germany). In this study, TRAP positive cell with no less than 3 nuclei was defined as osteoclast.

To investigate the resorption capability of osteoclasts on CPC tablets, the BMMs were seeded onto CPC tablets, incubated with differentiation medium for 5 days, and digested with 0.25% trypsin containing EDTA in PBS (pH = 7.2). The collected cells were re-seeded onto bone slices and incubated for another 2 days with differentiation medium. After that, the cells were treated with TRAP staining kit and observed with microscope as described above.

5.7. TRAP activity

After 7 days of incubation with differentiation medium, BMMs on CPC tablets were collected for TRAP activity analysis using TRAP enzyme assay kit (Sigma, USA) according to the manufacturer's instructions. The activity of enzyme was detected at 405 nm with plate reader (spectra MAX M2, Molecular Devices, USA). And the total protein concentration was determined by BCA Protein Assay Kit (Beyotime, China) to normalize the expression of TRAP enzyme.

5.8. Immunofluorescence analysis

Immunofluorescence analysis of incubated cells was conducted as follows: At the end of incubation, CPC scaffolds with cells were rinsed with PBS (pH = 7.2) for thrice and fixed with 4% paraformaldehyde for 10 min at room temperature. Then, 0.1% Triton X-100 was utilized for 15 min to make the cytomembrane permeable. Subsequently, the samples were incubated with mouse monoclonal RANK antibody (1:100 dilution; Santa Cruz, USA) was utilized and incubated for 12 h at 4 °C after blocking with 5% goat serum for 1 h, followed by 45-min incubation with AF-594-conjugated goat anti-mouse second antibody (1:500 dilution; Abcam, UK). FITC-Phalloidin (5 mg mL^{-1}, Thermo, USA) and DAPI (5 mg mL^{-1}, Sigma-Aldrich, USA) were used to counterstain cytoskeleton and nuclei, respectively. The images were obtained by CLSM (Nikon A1R, Japan). Some CPC tablets with cells were stained with FITC-Phalloidin and DAPI only for recognition of osteoclasts.

5.9. Cell morphology and resorption pits observation

SEM was utilized for the observation of cellular morphology on CPC tablets and resorption pits on bone slices. Briefly, at the end of induction, the cells on CPC tablets were fixed with 4% paraformaldehyde for 24 h at ambient temperature. And the cells on bone slices were removed to observe resorption pits. The cell-removing methods are as follows: the bone slices were soaked into 1 M ammonium hydroxide for 3min, subsequently, bone slices were cleaned ultrasonically for 10 min and fixed with 4% paraformaldehyde for 10 min at room temperature. Cell-detached bone slices and CPC tablets with cells were treated with ascending concentrations of ethanol as described above. Then the images of cells on CPC surface and resorption pits were collected by SEM (S-4800, Hitachi, Japan). Relative pits area was quantified by Image Pro 5.0 (Media Cybernetic, USA).

5.10. Transwell assays

To investigate the effect of ions released from CPC on osteoclast differentiation and function, 24-well Transwell plates (3472, Corning, USA) with 0.4-μm pore filters allowing the ions to pass by were applied. Briefly, the BMMs were seeded on bone slices placed in the lower chamber, and CPC tablet was placed in the upper chamber. Followed by the incubation with differentiation medium for 7 days, after which, the cells on bone slices were removed and the resorption pits were evaluated by SEM aforementioned. At the end of incubation, the supernatant was collected for TGF-β1 detection.

5.11. ELISA assays

After 1 day of incubation with differentiation medium, BMMs on CPC tablets were collected for RANK analysis. Briefly, the extracts of total protein were acquired by lysing cells on CPC tablets in cold radioimmunoprecipitation assay (RIPA) buffer (Beyotime, China). The concentration of RANK was measured by Mouse RANK ELISA Kit (Boster Biological Technology, China), according to the manufacturer's instructions and the total protein concentration was measured by BCA Protein Assay Kit (Beyotime, China), which was used to normalize the expression of RANK.

In transwell assays, at the end of incubation, supernatant was collected for the detection of bovine derived TGF-β1 (bone slice was from bovine). The concentration of TGF-β1 was measured according to the manufacturer's instruction (USCN Life Science, Wuhan, China). Total protein was measured as mentioned above to normalize the expression of TGF-β1.

5.12. qRT-PCR analysis

Gene expression was analyzed quantitatively by real time PCR. BMMs were plated on 48-well plate, followed by incubating with CPC extract differentiation medium for 7 days. Prime Script RT reagent kit was used to reverse-transcribe the messenger RNA (mRNA) extracted from cells utilizing Trizol reagent (Takara, Japan) according to the manufacturer's instructions. The qRT-PCR was conducted on CFX96 Touch™ PCR detection system (Bio-Rad, USA). Briefly, the operating was set as follows: 95 °C for 30 s followed by 40 cycles of 95 °C for 5 s and 60 °C for 30 s, during which the fluorescence intensity was recorded. Primers were purchased from Shanghai Shenggong Bioengineering Co., Ltd and their sequences were listed in supplementary table S2. GAPDH was used as housekeeping gene. The data were analyzed using the comparative Ct ($2^{-\Delta\Delta Ct}$) method and represented as a fold change relative to the control. All samples were analyzed in triplicate.

5.13. Western blot analysis

Western blot analysis was deployed to examine the expression of NF-κB signaling as described previously. Briefly, after stimulating with extract differentiation medium for 15 min, the total protein extracts of BMMs were acquired by lysing cells in cold radioimmunoprecipitation assay (RIPA) buffer. Then, proteins were separated with 6% SDS-polyacrylamide gel electrophoresis (SDS-PAGE) at an equal

concentration, followed by transferring onto PVDF (polyvinylidene difluoride) membranes. The membranes were blocked by 5% bovine serum albumin (BSA) for 1 h, and then incubated with anti-p65 (1:1000, Cell Signaling Technology, USA), anti-p-p65 (1:1000, Cell Signaling Technology, USA) and anti-IκBα (1:1000, Cell Signaling Technology, USA). β-actin was utilized as a loading control. Chemiluminescence imaging system (Tanon, China) was used to visualize and photograph the protein bands.

5.14. SPR analysis

BIAcore T200 (GE healthcare, USA) was used to measure the affinity of RANK and RANKL according to the earlier protocol [63]. In brief, human-RANK (5 μg mL^{-1}, ARCO Biosystems, China) with running buffer (1 × HEPES, with 0.005% Tween-20, pH = 7.4) was captured on CM5 chip (GE healthcare) via anti-mouse antibody at a flow rate of 10 μL min^{-1} to reach a capture level of about 200 response units (RU). To record the signal of RANK-RANKL affinity, human-RANKL (50 nM, ARCO Biosystems, China) dissolved in each CPC extract was injected into the channel. RANKL dissolved in α-MEM medium was treated as control. Between assays, 10 mM Glycine-HCl (pH = 1.7) was employed to regenerate the chip. All operations were conducted at 25 °C, and the signals were captured as sensor grams, which were transformed into a 1:1 binding model by employing BIAevaluation software 3.0 (GE healthcare, USA).

5.15. Animal surgery

We prepared porous CPC scaffolds (Φ5 x 2 mm) for in *in vivo* experiment. All procedure were identical as mentioned above except the slurry preparation. During mixing, we incorporated NaCl granules with the size of 300–500 μm and 100 μL saturated NaCl solution into the mixture of TECP and DCPA. After 3 days of curing, the samples were immersed into purified water until total dissolution of NaCl granules to obtain porous CPC scaffolds.

The porosity of porous CPC scaffolds was measured as previously described [8]. We measured the porosity of scaffolds according to the Archimedes' principle equation:

$$\text{Porosity}\ (\%) = \frac{(W - D) \times 100\%}{(W - S)}$$

where W means the wet weight, D means the dry weight and S means the weight suspended in anhydrous ethonal. Average porosity was calculated from the tests of three samples.

All procedures were supervised by the Animal Research Committee of East China University of Science and Technology. Briefly, 8-week-old male SD rats (n = 36, Shanghai jiesijie experimental animal Co., Ltd, China) were anesthetized by injection of pentobarbital (Nembutal, 30 mg kg^{-1}) intraperitoneally. Subsequently, an about 1.5 cm sagittal incision on scalp was created to expose calvarium, and two critical-sized defects were made by employing a trephine bur (ϕ = 5 mm, RWD Life Science, China). Eventually, calvarial defects (ϕ = 5 mm) were created and randomly implanted with CPC scaffolds (Φ5 × 3 mm): 1.4CPC (n = 24), 1.5CPC (n = 24), 1.67CPC (n = 24). Among samples in each group, the specific analysis and allocation was as follows: the analysis of Micro-CT, sequential fluorescent labeling, and VG staining in turn (n = 6) , the detection of TGF-β1 (n = 6), OPN staining analysis (n = 6), and TRAP staining evaluation (n = 6). The samples used for *in vivo* experiments were sterilized through gamma radiation at 15 KGY before implanting.

5.16. Sequential fluorescent labeling experiment

To evaluate new bone formation, polychrome sequential fluorescent labeling was performed according to previous reports [64]. In brief, the rats were injected intraperitoneally with tetracycline hydrochloride (25 mg kg^{-1}, TE, Sigma, USA), calcein (20 mg kg^{-1}, CA, Sigma, USA), and alizarin reds (30 mg kg^{-1}, AL, Sigma, USA) at 3, 6 and 9 weeks post operation, severally.

5.17. Micro-computed tomography (micro-CT) analysis

At 12 weeks post-operation, micro-CT (Sky scan 1076, Bruker, Germany) was employed to examine the harvested skulls after being fixed in cold 4% paraformaldehyde. VG Studio software (Volume graphics, Germany) was served for visualizing the reconstructed 3D images. The calculation of trabecular thickness (Tb. Th), and the percentage of new bone volume relative to tissue volume (BV/TV) in the defects was conducted with its auxiliary software (Scanco Medical AG, Switzerland).

5.18. Histological, histomorphometric and immunofluorescence analysis

Firstly, the skulls of rats were dehydrated using gradient ethanol (from 70% to 100%) and embedded in polymethylmethacrylate (PMMA). The sagittal section was cut using a diamond circular saw system (300 CL, Exakt Advanced Technology GmbH, Germany) and polished by a grinding system (400 CS, Exakt Advanced Technology GmbH, Germany), after which the CLSM (Nikon A1R, Japan) was employed to visualize the fluorescence labeling of the sections. The yellow (TE), green (CA), and red (AL) areas represented the newly formed bone at 3, 6, and 9 weeks after implantation, severally. Then, the sections were treated with van Gieson's picro fuchsin (VG) staining and pictured by microscope (Dmi8, Leica, Germany). The areas of newly formed bone were quantified using Image Pro 5.0 (Media Cybernetic, USA).

Samples were decalcified after micro-CT scanning and histologically analyzed. 5-μm paraffin sections were collected from central aspects in the defect area for TRAP staining. The images were pictured with microscope (Dmi8, Leica, Germany) and quantified utilizing Image Pro (Media Cybernetic, USA).

For immunofluorescence analysis, rabbit anti-rat osteopontin (OPN, 1:200, Abcam, USA) antibody was used as primary antibody to stain frozen sections of each sample at 4 °C overnight. Subsequently, AF-594-conjugated goat anti-rabbit second antibody was used to conjugate primary antibody for 1 h at room temperature away from light. Anti-fade reagent (Cell Signaling Technology, USA) with DAPI was applied to mount the sections. The images were photographed by CLSM (Nikon, A1R, Japan).

5.19. ELISA assays for TGF-β1

At 12 weeks post-surgery, the harvested samples were dissected and ground with 1 mL of PBS (pH = 7.2) using an agate mortar. The samples were centrifuged at 4 °C and the supernatant was carefully collected. Subsequently, the level of TGF-β1 in the supernatant was quantified using a commercial TGF-β1 ELISA kit (RD system, USA) following the manufacture's instruction.

5.20. Statistical analysis

All data were shown with mean standard deviation (SD), and one-way ANOVA followed by Turkey's post hoc test was used to analyze the data. A statistical significance was recognized at $^{*}P < 0.05$, $^{**}P < 0.01$, and $^{***}P < 0.001$.

Declaration of competing interest

The authors declare no conflict of interest.

CRediT authorship contribution statement

Xiaogang Wang: Conceptualization, Data curation, Formal analysis,

Visualization, Writing – original draft. **Yuanman Yu:** Data curation, Writing – review & editing. **Luli Ji:** Methodology, Writing – review. **Zhen Geng:** Writing – review & editing. **Jing Wang:** Project administration, Supervision, Writing – review & editing. **Changsheng Liu:** Funding acquisition, Project administration.

Acknowledgements

This research was supported by National Natural Science Foundation of China for Innovative Research Groups (No.51621002), and the National Natural Science Foundation of China (No.31870953). This study was also supported by the 111 Project (B14018).

Appendix A. Supplementary data

Supplementary data to this article can be found online at https://doi.org/10.1016/j.bioactmat.2021.05.003.

References

[1] Y. Li, Y. Xiao, C. Liu, The horizon of materiobiology: a perspective on material-guided cell behaviors and tissue engineering, Chem. Rev. 117 (2017) 4376.
[2] S. Yao, X. Lin, Y. Xu, Y. Chen, R. Tang, Osteoporotic bone recovery by a highly bone-inductive calcium phosphate polymer-induced liquid-precursor, Adv. Sci. 6 (2019) 1900683.
[3] W. Hao, N. Eliaz, Z. Xiang, H.P. Hsu, M. Spector, L.W. Hobbs, Early bone apposition in vivo on plasma-sprayed and electrochemically deposited hydroxyapatite coatings on titanium alloy, Biomaterials 27 (2006) 4192–4203.
[4] P. Habibovic, J. Li, C. Valk, G. Meijer, P. Layrolle, C. Blitterswijk, K.D. Groot, Biological performance of uncoated and octacalcium phosphate-coated Ti6Al4V, Biomaterials 26 (2005) 23–36.
[5] A.Y. Clark, K.E. Martin, J.R. García, C.T. Johnson, A.J. García, Integrin-specific hydrogels modulate transplanted human bone marrow-derived mesenchymal stem cell survival, engraftment, and reparative activities, Nat. Commun. 11 (2020) 114.
[6] M.L.M. Martino, K. Maruyama, G.A. Kuhn, T. Satoh, O. Takeuchi, R. Müller, S. Akira, Inhibition of IL-1R1/MyD88 signalling promotes mesenchymal stem cell-driven tissue regeneration, Nat. Commun. 7 (2016) 11051.
[7] D. Nyoung Heo, Monika Hospodiuk, T. Ibrahim Ozbolat, Synergistic interplay between human MSCs and HUVECs in 3D spheroids laden in collagen/fibrin hydrogels for bone tissue engineering, Acta Biomater. 95 (2019) 348–356.
[8] Y. Ma, W. Zhang, Z. Wang, Z. Wang, Q. Xie, H. Niu, H. Guo, Y. Yuan, C. Liu, PEGylated poly(glycerol sebacate)-modified calcium phosphate scaffolds with desirable mechanical behavior and enhanced osteogenic capacity, Acta Biomater. 44 (2016) 110–124.
[9] J. Jochen, S.N. Verena, K. Jens, S. Eduard, A. Konstantinos, Complications after spacer implantation in the treatment of hip joint infections, Int. J. Med. Sci. 6 (2009) 265.
[10] X. Wu, K. Al-Abedalla, E. Rastikerdar, S.A. Nader, F. Tamimi, Selective serotonin reuptake inhibitors and the risk of osseointegrated implant failure: a cohort study, J. Dent. Res. 93 (2014) 1054–1061.
[11] C.M. Court-Brown, M.M. Mcqueen, Nonunions of the proximal humerus: their prevalence and functional outcome, J. Trauma Acute Care 64 (2008) 1517–1521.
[12] D.W. Sanders, R.D. Galpin, M. Hosseini, M.D. Macleod, Morbidity resulting from the treatment of tibial nonunion with the Ilizarov frame, Can. J. Surg. 45 (2002) 196–200.
[13] X. Lin, S. Patil, Y.-G. Gao, A. Qian, The bone extracellular matrix in bone formation and regeneration, Front. Pharmacol. 11 (2020) 757.
[14] N. Dirckx, M.C. Moorer, T.L. Clemens, R.C. Riddle, The role of osteoblasts in energy homeostasis, Nat. Rev. Endocrinol. 15 (2019) 651–665.
[15] J. Luo, Z. Yang, Y. Ma, Z. Yue, H. Lin, G. Qui, J. Huang, W. Dai, C. Li, C. Zheng, L. Xu, H. Chen, J. Wang, D. Li, S. Siwko, J.M. Penninger, G. Ning, J. Xiao, M. Liu, LGR4 is a receptor for RANKL and negatively regulates osteoclast differentiation and bone resorption, Nat. Med. 22 (2016) 539–546.
[16] A. Salhotra, H.N. Shah, B. Levi, M.T. Longaker, Mechanisms of bone development and repair, Nat. Rev. Mol. Cell Biol. 21 (2020) 696–711.
[17] W.J. Boyle, W.S. Simonet, D.L. Lacey, Osteoclast differentiation and activation, Nature 423 (2003) 337–342.
[18] Y.Y. Kong, H. Yoshida, I. Sarosi, H.L. Tan, E. Timms, C. Capparelli, S. Morony, A. J. Oliveira-dos-Santos, G. Van, A. Itie, W. Khoo, A. Wakeham, C.R. Dunstan, D. L. Lacey, T.W. Mak, W.J. Boyle, J.M. Penninger, OPGL is a key regulator of osteoclastogenesis, lymphocyte development and lymph-node organogenesis, Nature 397 (1999) 315–323.
[19] C.E. Jacome-Galarza, G.I. Percin, J.T. Muller, M. Elvira, L. Tomi, E. Jiri, R. Martina, V.K. Yadav, C. Lucile, B. Mathieu, Developmental origin, functional maintenance and genetic rescue of osteoclasts, Nature 568 (2019) 541–545.
[20] T.R. Arnett, I.R. Orriss, Metabolic properties of the osteoclast, Bone 115 (2018) 25–30.
[21] Y. Tang, X. Wu, W. Lei, L. Pang, C. Wan, Z. Shi, L. Zhao, T.R. Nagy, X. Peng, J. Hu, TGF-beta1-induced migration of bone mesenchymal stem cells couples bone resorption with formation, Nat. Med. 15 (2009) 757–765.
[22] H. Xie, Z. Cui, L. Wang, Z. Xia, Y. Hu, L. Xian, C. Li, L. Xie, J. Crane, M. Wan, PDGF-BB secreted by preosteoclasts induces angiogenesis during coupling with osteogenesis, Nat. Med. 20 (2014) 1270–1278.
[23] N.L. Davison, B. Ten Harkel, T. Schoenmaker, X. Luo, H. Yuan, V. Everts, F. Barrère-de Groot, J.D. De Bruijn, Osteoclast resorption of beta-tricalcium phosphate controlled by surface architecture, Biomaterials 35 (2014) 7441–7451.
[24] N.L. Davison, J. Su, H. Yuan, J.J.V.D. Beucken, B.D. Groot, Influence of surface microstructure and chemistry on osteoinduction and osteoclastogenesis by biphasic calcium phosphate discs, Eur. Cell. Mater. 29 (2015) 314–329.
[25] V. Uskoković, I. Janković-Častvan, V.M. Wu, Bone mineral crystallinity governs the orchestration of ossification and resorption during bone remodeling, ACS Biomater. Sci. Eng. 5 (2019) 3483–3498.
[26] M. Lotz Ethan, Michael B. Berger, Zvi Schwartz, Barbara Boyan, Regulation of osteoclasts by osteoblast lineage cells depends on titanium implant surface properties, Acta Biomater. 68 (2018) 296–307.
[27] Yukari Shiwaku, Lynn Neff, Kenichi Nagano, Ken-Ichi Takeyama, de Joost, The Crosstalk between Osteoclasts and Osteoblasts is dependent upon the composition and structure of biphasic calcium phosphates, PloS One 10 (2015), 0132903.
[28] P.J. Marie, Strontium as therapy for osteoporosis, Curr. Opin. Pharmacol. 5 (2005) 633–636.
[29] B. Li, P. Gao, H. Zhang, Z. Guo, Y. Zheng, Y. Han, Osteoimmunomodulation, osseointegration, and in vivo mechanical integrity of pure Mg coated with HA nanorod/pore-sealed MgO bilayer, Biomater. Sci. 6 (2018) 3202–3218.
[30] C. Capuccini, P. Torricelli, E. Boanini, M. Gazzano, R. Giardino, A. Bigi, Interaction of Sr-doped hydroxyapatite nanocrystals with osteoclast and osteoblast-like cells, J. Biomed. Mater. Res. 89 (2010) 594–600.
[31] J. Ren, K.A. Blackwood, A. Doustgani, P.P. Poh, R. Steck, M.M. Stevens, M. A. Woodruff, Melt-electrospun polycaprolactone strontium-substituted bioactive glass scaffolds for bone regeneration, J. Biomed. Mater. Res. 104 (2016) 2109.
[32] Li Jingfeng, Liu Xifeng, Park Sungjo, Miller Lee, Andre, Strontium-substituted hydroxyapatite stimulates osteogenesis on poly(propylene fumarate) nanocomposite scaffolds, J. Biomed. Mater. Res. 107 (2018) 631–642.
[33] E. Gentleman, Y.C. Fredholm, G. Jell, N. Lotfibakhshaiesh, M.D. O'Donnell, R. G. Hill, M.M. Stevens, The effects of strontium-substituted bioactive glasses on osteoblasts and osteoclasts in vitro, Biomaterials 31 (2010) 3949–3956.
[34] Liu Wei, Li Jinhua, Cheng Mengqi, Wang Qiaojie, Kelvin, Zinc-modified sulfonated polyetheretherketone surface with immunomodulatory function for guiding cell fate and bone regeneration, Adv. Sci. 5 (2018), 1800749.
[35] W. Fei, L. Guanqi, G. Yuanlong, C.R. William, C. Zetao, X. Yin, Blood prefabricated hydroxyapatite/tricalcium phosphate induces ectopic vascularized bone formation via modulating the osteoimmune environment, Biomater. Sci. 6 (2018) 2156–2171.
[36] A. Mansour, L. Abu-nada, H. Al-Waeli, M.A. Mezour, M.N. Abdallah, J.M. Kinsella, J. Kort-Mascirt, J.E. Henderson, J.L. Ramirez-Garcialuna, S.D. Tran, O.A. Elkashty, A. Mousa, A.A. Ei-Hadad, D. Taqi, F. Al-Hamad, O. Alageel, M.T. Kaartinen, F. Tamimi, Bone extracts immunomodulate and enhance the regenerative performance of dicalcium phosphates bioceramics, Acta Biomater. 89 (2019) 343–358.
[37] A. Diez-Escudero, E. Torreggiani, G.D. Pompo, M. Espanol, C. Persson, G. Ciapetti, N. Baldini, M.-P. Ginebra, Effect of calcium phosphate heparinization on the in vitro inflammatory response and osteoclastogenesis of human blood precursor cells, J. Tissue Eng. Regen. M. 13 (2019) 1217–1229.
[38] S. Hirayama, S. Takagi, M. Markovic, L.C. Chow, Properties of calcium phosphate cements with different tetracalcium phosphate and dicalcium phosphate anhydrous molar ratios, J. Res. Natl. Inst. Stan. 113 (2008) 311–320.
[39] T. Matsubara, T. Yaginuma, W.N. Addison, Y. Fujita, S. Kokabu, Plectin stabilizes microtubules during osteoclastic bone resorption by acting as a scaffold for Src and Pyk2, Bone 132 (2019) 115209.
[40] T. Julia Warren, Wei Zou, E. Corinne Decker, Rohatgi Nidhi, A. Christopher Nelson, Correlating RANK ligand/RANK binding kinetics with osteoclast formation and function, J. Cell. Biochem. 116 (2015) 2476–2483.
[41] M. Inoue, M.L. Shinohara, Intracellular osteopontin (iOPN) and immunity, Immunol. Res. 49 (2011) 160–172.
[42] K. Anai, A. Matthew, C. Victor, B. Robert, S. Wing-Kin, Z. Jiwang, M. Zhiyong, K. Paul, Osteopontin—a master regulator of epithelial-mesenchymal transition, J. Clin. Med. 5 (2016) 39.
[43] C. Comi, M. Carecchio, A. Chiocchetti, S. Nicola, D. Galimberti, C. Fenoglio, G. Cappellano, F. Monaco, E. Scarpini, U. Dianzani, Osteopontin is increased in the cerebrospinal fluid of patients with alzheimer's disease and its levels correlate with cognitive decline, J. Alzheimers Dis. 19 (2010) 1143–1148.
[44] Q. Ge, D.W. Green, D.J. Lee, H.Y. Kim, Z. Piao, J.M. Lee, H.S. Jung, Mineralized polysaccharide transplantation modules supporting human MSC conversion into osteogenic cells and osteoid tissue in a non-union defect, Mol. Cells 41 (2018) 1016–1023.
[45] R. Agarwal, A.J. García, Biomaterial strategies for engineering implants for enhanced osseointegration and bone repair, Adv. Drug Deliv. Rev. 94 (2015) 53–62.
[46] J. Lan, Z.F. Wang, B. Shi, H.B. Xia, X.R. Cheng, The influence of recombinant human BMP-2 on bone-implant osseointegration: biomechanical testing and histomorphometric analysis, Int. J. Oral Maxillofac. Surg. 36 (2007) 345–349.
[47] L. Maimoun, T.C. Brennan, I. Badoud, V. Dubois-Ferriere, R. Rizzoli, P. Ammann, Strontium ranelate improves implant osseointegration, Bone 46 (2010) 1436–1441.
[48] M. Schumacher, A.S. Wagner, J. Kokesch-Himmelreich, A. Bernhardt, M. Rohnke, S. Wenisch, M. Gelinsky, Strontium substitution in apatitic CaP cements effectively

attenuates osteoclastic resorption but does not inhibit osteoclastogenesis, Acta Biomater. 37 (2016) 184–194.
[49] N. Kanatani, T. Sugimoto, N. Kanzawa, S. Yano, K. Chihara, High extracellular calcium inhibits osteoclast-like cell formation by directly acting on the calcium-sensing receptor existing in osteoclast precursor cells, Biochem. Bioph. Res. Co. 261 (1999) 144–148.
[50] M. Kanatan, T. Sugimoto, J. Kano, M. Kanzawa, K. Chihara, Effect of high phosphate concentration on osteoclast differentiation as well as bone-resorbing activity, J. Cell. Physiol. 196 (2003) 180–189.
[51] H.R. Bosshard, D.N. Marti, I. Jelesarov, Protein stabilization by salt bridges: concepts, experimental approaches and clarification of some misunderstandings, J. Mol. Recogn. 17 (2004) 1–16.
[52] C.A. Nelson, J.T. Warren, M.W.H. Wang, S.L. Teitelbaum, D.H. Fremont, RANKL employs distinct binding modes to engage RANK and the osteoprotegerin decoy receptor, Structure 20 (2012) 1971–1982.
[53] V.M. Wu, V. Uskoković, Is there a relationship between solubility and resorbability of different calcium phosphate phases in vitro? Biochim. Biophys. Acta 1860 (2016) 2157–2168.
[54] C. Liu, W. Shen, Y. Gu, L. Hu, Mechanism of the hardening process for a hydroxyapatite cement, J. Biomed. Mater. Res. 35 (1997) 75–80.
[55] M. Bohner, R.J. Miron, A proposed mechanism for material- induced heterotopic ossification, Mater. Today 22 (2019) 132–141.
[56] V. Iotsova, J. Caamaño, J. Loy, Y. Yang, A. Lewin, R. Bravo, Osteopetrosis in mice lacking NF-|[kappa]|B1 and NF-|[kappa]|B2, Nat. Med. 3 (1997) 1285–1289.
[57] Z. Liu, K.B. Mar, N.W. Hanners, S.S. Perelman, M. Kanchwala, C. Xing, J. W. Schoggins, N.M. Alto, A NIK–SIX signalling axis controls inflammation by targeted silencing of non-canonical NF-κB, Nature 568 (2019) 249–253.
[58] L.H. Xia, J. Kilb, H. Wex, Z.Q. Li, A. Lipyansky, V. Breuil, L. Stein, J.T. Palmer, D. W. Dempster, D. Bromme, Localization of rat cathepsin K in osteoclasts and resorption pits: inhibition of bone resorption and cathepsin K-activity by peptidyl vinyl sulfones, Biol. Chem. 380 (1999) 679–687.
[59] R. Agarwal, A. García, Biomaterial strategies for engineering implants for enhanced osseointegration and bone repair, Adv. Drug Deliv. Rev. 94 (2015) 53–62.
[60] T. Histing, C. Anton, C. Scheuer, P. Garcia, J.H. Holstein, M. Klein, R. Matthys, T. Pohlemann, M.D. Menger, Melatonin impairs fracture healing by suppressing RANKL-mediated bone remodeling, J. Surg. Res. 173 (2012) 83–90.
[61] T. Histing, D. Stenger, C. Scheuer, W. Metzger, P. Garcia, J.H. Holstein, M. Klein, T. Pohlemann, M.D. Menger, Pantoprazole, a proton pump inhibitor, delays fracture healing in mice, Calcif. Tissue Int. 90 (2012) 507–514.
[62] J. Zhang, X. Ma, D. Lin, H. Shi, Y. Yuan, W. Tang, H. Zhou, H. Guo, J. Qian, C. Liu, Magnesium modification of a calcium phosphate cement alters bone marrow stromal cell behavior via an integrin-mediated mechanism, Biomaterials 53 (2015) 251–264.
[63] S. Zhang, C. Liu, P. Huang, S. Zhou, J. Ren, Y. Kitamura, P. Tang, Z. Bi, B. Gao, The affinity of human RANK binding to its ligand RANKL, Arch. Biochem. Biophys. 487 (2009) 49–53.
[64] D. Lin, Y. Chai, Y. Ma, D. Bing, Y. Yuan, C. Liu, Rapid initiation of guided bone regeneration driven by spatiotemporal delivery of IL-8 and BMP-2 from hierarchical MBG-based scaffold, Biomaterials 196 (2019) 122–137.